Petroleum Science 19 (2022) 441–458

Contents lists available at ScienceDirect

Petroleum Science

journal homepage: www.keaipublishing.com/en/journals/petroleum-science

Original Paper

Assessment of recoverable oil and gas resources by in-situ conversion of shale—Case study of extracting the Chang 7_3 shale in the Ordos Basin

Lian-Hua Hou [a, b, *], Xia Luo [a], Sen-Hu Lin [a], Yong-Xin Li [a, **], Li-Jun Zhang [a], Wei-Jiao Ma [c]

[a] Research Institute of Petroleum Exploration & Development, PetroChina, Beijing, 100083, China
[b] National Energy Tight Oil & Gas R&D Center, Beijing, 100083, China
[c] School of Geosciences, China University of Petroleum, Qingdao, Shandong, 266580, China

ARTICLE INFO

Article history:
Received 14 November 2020
Accepted 15 July 2021
Available online 23 October 2021

Edited by Jie Hao

Keywords:
Shale oil
In-situ conversion processing
Thermal simulation experiment
Hydrocarbon generation mechanism
Hydrocarbon resource
Ordos basin

ABSTRACT

The purpose of this study is to investigate the entire evolution process of shales with various total organic contents (TOC) in order to build models for quantitative evaluation of oil and gas yields and establish methods for assessing recoverable oil and gas resources from in-situ conversion of organic matters in shale. Thermal simulation experiments under in-situ conversion conditions were conducted on Chang 7_3 shales from the Ordos Basin in a semi-open system with large capacity. The results showed that TOC and R_o were the key factors affecting the in-situ transformation potential of shale. The remaining oil and gas yields increased linearly with TOC but inconsistently with R_o. R_o ranged 0.75%−1.25% and 1.05%−2.3%, respectively, corresponding to the main oil generation stage and gas generation stage of shale in-situ transformation. Thus a model to evaluate the remaining oil/gas yield with TOC and R_o was obtained. The TOC of shale suitable for in-situ conversion should be greater than 6%, whereas its R_o should be less than 1.0%. Shales with 0.75% (R_o) could obtain the best economic benefit. The results provided a theoretical basis and evaluation methodology for predicting the hydrocarbon resources from in-situ conversion of shale and for the identification of the optimum "sweet spots". The assessment of the Chang 7_3 shale in the Ordos Basin indicated that the recoverable oil and gas resources from in-situ conversion of organic matters in shale are substantial, with oil and gas resources reaching approximately 450×10^8 t and 30×10^{12} m^3, respectively, from an area of 4.27×10^4 km^2.

1. Introduction

With the future increase in the global population and economy, the energy demand will grow substantially in the next few decades (Ma et al., 2020a). The global oil consumption has already risen from 41.43×10^8 t in 2008 to 46.62×10^8 t in 2018 (BP, 2019). Energy security has drawn the attention of many countries to their oil and gas supply. The successful development of shale oil and gas in the US has reshaped the energy landscape in the world (Jia et al., 2012; Zendehboudi and Bahadori et al., 2017; Yang and Zou et al., 2019; Zhao et al., 2020). In 2019, the crude oil production reached 44.65 billion barrels in the US, of which, 29.14 billion barrels were from shale oil, accounting for 65.12% of the total oil production that year (EIA, 2020−01). Shale oil is playing an increasingly important role in the dramatic growth of American oil production (EIA, 2018, 2019a, 2019b; Zhou et al., 2019; Zou et al., 2019) and exerts a significant influence on the global energy and geopolitical layout.

The technologies of horizontal wells and multi-stage fracturing have driven the rapid growth of oil and gas production from shales with medium-high maturity in the US (IHS, 2016; Jin et al., 2019a; Perrin, 2019-06-06). Consequently, China has attached great importance to shale oil and gas (Zou et al., 2010; Lu et al., 2012; Xue et al., 2015; Du et al., 2019; Ju et al., 2020; Kuang et al., 2020; Song et al., 2020). Surveys indicate that two types of shale, i.e., lacustrine

* Corresponding author. Research Institute of Petroleum Exploration & Development, PetroChina, Beijing, 100083, China.
** Corresponding author.
E-mail addresses: houlh@petrochina.com.cn (L.-H. Hou), lyxin@petrochina.com.cn (Y.-X. Li).

https://doi.org/10.1016/j.petsci.2021.10.015

shale and marine shale, are developed in China. Marine shales are mainly distributed in South China with relatively high maturity, in which the vitrinite reflectance (R_o) is generally greater than 2.0% (Zou et al., 2011, 2015; Zhao et al., 2012, 2016; Nie et al., 2016). These areas contain abundant shale gas resources and some have been developed successfully with a production of 150×10^8 m^3 in 2019. However, lacustrine shales are primarily distributed in North China, including the Ordos, Songliao, Bohai Bay and Junggar Basins, covering an area of more than 20×10^4 km^2 (Dang et al., 2015; Zhao et al., 2018a,b; Yang and Jin, 2019; Zou et al., 2020) and characterized by relatively low maturity for which the R_o is normally less than 1.0%. China has been attempting to exploit the shale oil in its lacustrine formations for more than a decade by drilling nearly 500 horizontal wells. However, the economic development of shale oil with low and medium maturity has not yet been realized, and the undeveloped organic pores, poor connectivity, low gas-oil ratio (GOR) and high viscosity of oil are the main reasons, all of which lead to an extremely low recovery factor of only 1%–3% (Saif et al., 2017; Jin et al., 2019b; Hou et al., 2020a) by simply relying on volume fracturing in horizontal wells. Prospecting history in the US also shows that conventional volume fracturing in horizontal wells is unable to realize the economic development of shale oil with low to medium maturity. Instead, in-situ conversion must be used to achieve economic development. Shell, ExxonMobil, Total, and many other giant oil companies have conducted relevant research and established four types of in-situ heating technologies, including electric heating, convection heating, radiant heating, and combustion heating (Wang et al., 2013).

In-situ conversion of shale oil, including physical and chemical process, enables the organic matter (including solid organic matter and asphalt) in shale or oil shale to be rapidly converted into light oil and natural gas by in-situ heating. It is then exploited, while coke and other residues are left in the subsurface. This process can be regarded as an "underground refinery" (Zhao et al., 2018a,b). In-situ transformation of shale has four technical advantages: (1) the oil obtained through the in-situ heating and conversion is of good quality (35–49° API); (2) the overpressure fluid and micro-fracture network generated by the in-situ conversion process increase the driving force, the permeable channels, and the drainage system, resulting in an ultimate recovery surpassing 60%; (3) there are no tailings or waste produced, with little groundwater pollution and no hydraulic fracturing needed, which attains actual clean mining by minimizing the damage to the ecosystem caused by harmful byproducts during conventional production; and (4) the occupied area is very small, which helps to protect farmland. The in-situ conversion technologies can successfully tackle the challenges in exploiting the shale with low-medium maturity, and lead to efficient and environmentally friendly utilization (hereafter we use shale to represent both the shale and oil shale). Nonetheless, some key issues must be addressed to achieve commercial development of the shale oil with low-medium maturity, including but not limited to criteria for the selection and evaluation of the recovery targets. To address these issues, we took the shale of the 3rd section in the Chang 7 member of the Tertiary in the Ordos Basin (hereafter referred to as the Chang 7_3 shale) as an example to simulate the hydrocarbon generation and expulsion process under in-situ conditions with a semi-open system. The purpose was to establish an approach with which to evaluate the recoverable oil and gas resources from in-situ conversion of shale, to provide a theoretical basis and evaluation methodology for predicting the hydrocarbon resources from in-situ conversion of shale, and to identify the optimum "sweet spots."

2. Samples and experimental conditions

2.1. Samples

The Chang 7_3 shale developed in the Late Triassic sediment in semi-deep to deep lacustrine facies. It is characterized by continuous sedimentation with large thickness, high organic matter abundance (average total organic content (TOC) is 14.32 wt%), and a good organic matter type (TypeII kerogen (Ma et al., 2020b; Hou et al., 2020b)). A series of hydrocarbon generation and expulsion thermal simulations were conducted by analyzing various Chang 7_3 shale outcrop samples with different TOC values. Altogether, nine samples were acquired from 5 m below the surface (to avoid the effects of epigenesis, such as weathering and leaching) in the southeast of the Ordos Basin (Fig. 1). The R_o of the samples was less than 0.5%. The samples were crushed into 40–60 mesh size, mixed, and divided evenly into several parts. Then, some samples were randomly chosen for TOC, Rock-Eval, and vitrinite reflectance (R_o) tests to obtain fundamental geochemical information (see Table 1).

2.2. Experimental device and process

Pyrolysis experiment is one of the most direct and efficient ways to investigate the oil and gas generation process. Previous researchers have conducted a large number of simulation studies by changing experimental conditions, including the sample feed (from 10 mg (You et al., 2019) to 200 g (Tang et al., 2015)), heating rate (from 0.5 to 25 °C/s to 12 °C/h (Doan et al., 2013; Lan et al., 2015; Siramard et al., 2017), pyrolysis temperature (max temperature from 420 °C (Siramard et al., 2017; Ma et al., 2020c) to 1000 °C (Shao et al., 2019)), and pressure (0.06–68 MPa (Lan et al., 2015; Sun et al., 2019; Yan et al., 2019)). Based on these studies, kinetic models have been built of hydrocarbon generation of different types of organic matter (Han et al., 2014), impacts of temperature and pressure on hydrocarbon generation have been discussed, and it was concluded that a rapid heating rate reduces oil generation, increase gas generation (Siramard et al., 2017), and exerts very little influence on the kinetic parameters (Bai et al., 2015). Thermal simulation experiments deepen our understanding of the hydrocarbon generation process. However, they also have disadvantages like other technologies. For instance, the error in assessing oil and gas generation can increase if the sample feed is small, and the heating rate is rapid. Additionally, there has not been much discussion regarding the oil and gas expulsion process constrained by experimental instruments. In this paper, thermal simulations with large sample feed and a slow heating rate were designed in a semi-open system using newly developed reactors with a large capacity. A total of 99 experiments were completed with nine samples at 11 temperatures to study the hydrocarbon generation features of the low maturity shale with various TOC values.

The experimental devices are diagramed in Fig. 2. The reactor was made of a special alloy, resistant to corrosion by H_2S, CO_2, and H_2. A special gasket and coating were used between the reactor body and cap to ensure long-term operation without leakage. The highest temperature that the reactor could bear was 700 °C, the maximum pressure was 40 MPa, the container capacity was 1.36 L, and samples weighing approximately 2 kg could be accommodated. The instrument meets the experimental requirements of thermal simulation of large-volume shale under different temperatures and pressures. The reactor has two heating systems, one at the bottom and the other on the side. They can operate simultaneously. Additionally, multiple thermocouples and pressure

Fig. 1. Shale distribution in the Ordos Basin and the sampling point.

Table 1
Basic geochemical data of the original unheated shale samples.

	No. 1[a]	No. 2	No. 3	No. 4	No. 5	No. 6	No. 7	No. 8	No. 9
TOC, wt.%	0.51	2.03	3.50	5.03	6.44	8.51	13.34	20.67	25.99
S_1, mg/g original rock	0.08	0.32	0.62	0.85	1.31	1.70	2.79	4.48	5.59
S_2, mg/g original rock	1.99	8.60	17.28	24.53	32.06	42.42	67.17	111.95	138.20
T_{max}, °C	435	433	429	432	431	433	429	428	427
HI, mg/g·TOC	388.1	423.0	494.5	487.9	498.2	498.6	503.5	541.5	531.8
R_o, %	0.43	0.46	0.47	0.47	0.47	0.47	0.48	0.47	0.48

[a] No. 1-No. 9 represent nine samples.

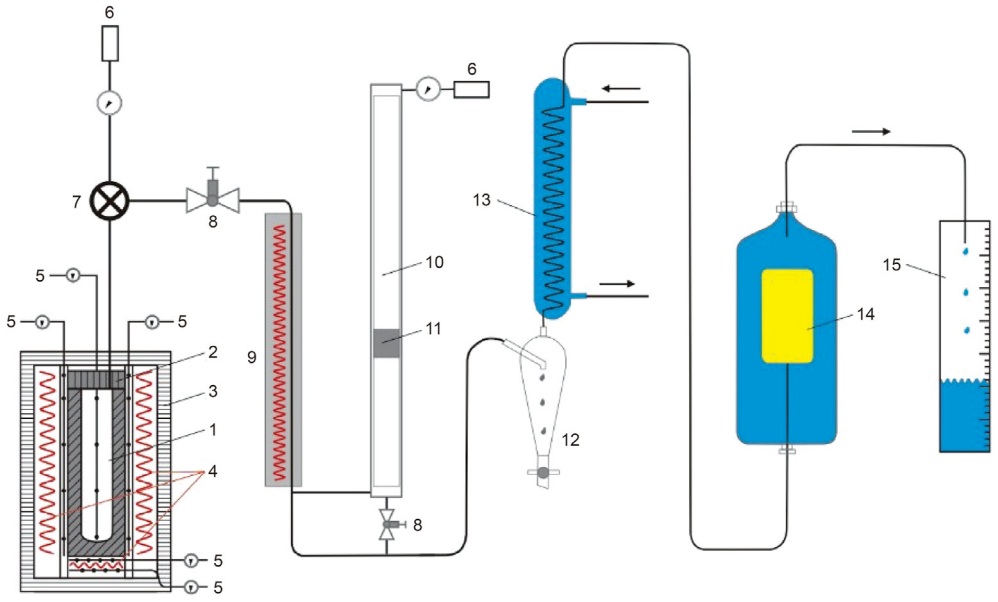

Fig. 2. Schematic diagram of the pyrolysis device. (1) autoclave, (2) sealing cover, (3) outer cover, (4) electric heater, (5) thermo couple, (6) pressure meter, (7) piston valve controlled by three-way solenoid valve, (8) needle valve, (9) heating tape, (10) synchronous collector, (11) floating piston, (12) liquid collector, (13) condenser, (14) gas bag, (15) measuring cylinder.

Table 2
Characteristics of the residual samples after pyrolysis experiments.

Pyrolysis Temperature, °C	Sample number																		Average R_o, %
	No. 1		No. 2		No. 3		No. 4		No. 5		No. 6		No. 7		No. 8		No. 9		
	TOC, %	R_o, %	TOC, %	R_o, %	TOC, %	R_o, %	TOC, %	R_o, %	TOC, %	R_o, %	TOC, %	R_o, %	TOC, %	R_o, %	TOC, %	R_o, %	TOC, %	R_o, %	
250	0.51	0.57	2.02	0.55	3.47	0.59	5.02	0.56	6.43	0.59	8.45	0.59	13.25	0.58	20.54	0.57	25.82	0.60	0.58
300	0.48	0.78	1.87	0.72	3.18	0.76	4.63	0.78	5.85	0.72	7.75	0.78	12.11	0.75	18.92	0.79	23.54	0.75	0.76
320	0.44	0.80	1.73	0.88	2.96	0.81	4.24	0.84	5.44	0.86	7.21	0.84	11.17	0.85	17.32	0.84	21.27	0.82	0.84
335	0.37	0.95	1.39	0.93	2.37	0.88	3.44	0.88	4.37	0.92	5.80	0.90	8.99	0.91	13.48	0.93	16.98	0.89	0.91
350	0.31	0.98	1.18	1.00	1.97	1.03	2.88	0.99	3.68	0.96	4.78	0.97	7.48	1.01	11.51	0.99	14.38	1.02	1.00
360	0.30	1.09	1.12	1.10	1.76	1.09	2.56	1.03	3.23	1.07	4.45	1.10	6.80	1.03	10.29	1.06	12.60	1.05	1.07
390	0.33	1.26	1.30	1.23	2.11	1.21	2.97	1.22	3.78	1.28	5.01	1.29	7.64	1.24	11.75	1.23	14.84	1.22	1.24
440	0.37	1.68	1.37	1.70	2.20	1.67	3.14	1.63	4.00	1.65	5.22	1.70	8.16	1.68	12.12	1.68	15.07	1.67	1.67
500	0.38	2.41	1.41	2.41	2.25	2.41	3.20	2.41	4.12	2.37	5.38	2.34	8.21	2.30	12.18	2.27	15.17	2.30	2.36
540	0.38	2.88	1.40	3.00	2.20	2.94	3.29	2.88	4.14	2.94	5.41	2.97	8.22	2.94	12.26	2.94	15.28	2.88	2.93
580	0.38	3.76	1.39	3.76	2.26	3.72	3.25	3.76	4.16	3.76	5.47	3.68	8.34	3.76	12.29	3.61	15.32	3.65	3.72

sensors are equipped to precisely control the temperature and pressure inside the reactor, such that the temperature error is below 1 °C and the fluid pressure error is less than 0.1 MPa during experiments.

The experimental steps are discussed below.

(1) Sample loading. The crushed and evenly mixed shale samples were loaded to the reactor.

(2) Heating simulation. ① Leak test. After sealing the reactor, vacuumed it, filled it with 20 MPa helium, and placed it for leak test. When there was no leakage, released the gas. Repeated the process for 3–4 times, and vacuumized the reactor for the last time. ② Heating. 5 MPa and 7 MPa were set as the fluid pressure and hydrocarbon expulsion pressure respectively. A total of 11 thermal simulation temperature points were designed (Table 2), covering the whole process of oil and gas generation. The heating procedure was as

follows: the sample was heated from room temperature to the temperature before each set point at the heating rate of 20 °C/d (the temperature before the first temperature point is 200 °C), and then the sample was heated to the set temperature at the heating rate of 5 °C/d, and kept at this temperature for 10 h.

(3) Simulation, product collection and quantification. ① hydrocarbon expulsion. The process of hydrocarbon expulsion was controlled by the three-way solenoid valve. At the beginning, the piston valve was closed and the whole reactor was sealed. When the generated products accumulated continuously in the container and the fluid pressure exceeded the set value, the piston valve would open automatically, and the products were released from the top of the reactor until the pressure dropped to the preset value. After that, the piston valve would close automatically and the reactor would be closed again. ② Collection and quantification of pyrolysis products. When products were discharged, their release rate was controlled by the needle valve, so that the pressure in the container was not reduced rapidly, and the synchronous collector could also play a buffer role, so as to ensure that the oil and gas could be separated in time when they were generated and discharged in large quantities. The hydrocarbon expulsion pipeline in the apparatus was wrapped with a heating belt, and the temperature of the heating belt was synchronized with the temperature in the reactor to prevent the condensation of products from blocking the pipeline. When the product passed through the condenser (water circulation at 20 °C), water and hydrocarbon liquid (including C_5) were collected in the liquid collector. Hydrocarbon gas (C_1–C_4) and non-hydrocarbon gas were collected in the air bag immersed in the water tank. The volume of the gas bag was determined by the volume of water discharged from the expansion of the air bag. Comparing the mass or volume of produced oil or gas before thermal simulation, the oil and gas yields of shale sample could be obtained. ③ Collection and quantification of retained oil and solid residual sample. After the autoclave cooled down to room temperature, the simulated source rock sample was taken out, weighed and extracted with dichloromethane, which was regarded as retained oil. The gas obtained by purging was the retained gas (the retained oil and gas were not discussed here, as they were not involved in our product modelling). The residual samples were tested for TOC and R_o after dichloromethane extraction (Table 2).

(4) Reliability analysis of simulation results. Theoretically, the mass of the reactants before and after the thermal simulation was conserved. Nevertheless, measurement errors and equipment leakage may cause product loss and result in disequilibrium. The mass balance rate, the ratio of the product mass after simulation (including oil, gas, water, and residuals) to that of the shale sample before simulation, was used to evaluate the reliability of the experimental results (Equation (1)).

$$\text{Mass balance} = \frac{\text{residual rock} + \text{oil} + \text{water} + \text{gas}}{\text{unheated rock}} \times 100\% \quad (1)$$

where mass balance is the mass balance rate, residual rock is the mass of the residual sample after simulation, oil is the mass of the produced and remaining oil after simulation, water is the mass of the produced and remaining water after simulation, gas is the mass of the produced and remaining gas after simulation, and unheated rock is the mass of the sample in the reactor before simulation.

The mass balance rate should be no less than 99.5% if there is only a measurement error. Otherwise, leakage occurred during the simulation and the results are not reliable. Under such circumstances, the thermal simulation must be conducted again. In this study, the mass balance rates of all 99 simulations exceeded 99.75% (Fig. 3), indicating the results of the pyrolysis experiments were reliable.

3. Experimental results

3.1. Relationship between pyrolysis and R_o

Thermal maturity is an important parameter with which hydrocarbon generation and expulsion (Tissot and Welte, 1984) can be assessed. Of the various evaluation indexes, R_o is the only indicator put forward as an international measurement standard (Stach et al., 1982) and is widely used. The R_o of the residual samples at each simulation temperature was analyzed, and the results indicated that there were very highly positive correlations between R_o and temperature was analyzed, and the results indicated that there were very highly positive correlations between R_o and the thermal simulation temperature (Fig. 4). Furthermore, the measured R_o values of different samples at the same temperature were very close. Therefore, the average R_o of the nine samples at each temperature was used to establish the model to express the relationship between thermal simulation temperature and R_o (Equation (2)).

$$R_o = a_1 \times e^{a_2 T} \quad (2)$$

where R_o is vitrinite reflectance, T is thermal simulation temperature, and a_1 and a_2 are empirical coefficients, equal to 0.1380 and 0.0057, respectively.

3.2. Characteristics of hydrocarbon yield from in-situ conversion of shale

Fig. 5 shows the yields of oil and gas with increasing R_o. Generally, the oil and gas yields of shale increased linearly with TOC, that was, the higher the abundance of organic matter (TOC) in source rock, the higher the yields. For example, the oil and gas yields of the sample with TOC of 25.988 wt% are 66.85 mg/g·rock and 33.30 mL/g·rock at $R_o = 3.65\%$. However, the variation trend of oil and gas yields were different from that of R_o. For oil yield, it increased rapidly at the beginning of thermal evolution and reached the peak of oil generation at $R_o \approx 1.2\%$, which was similar with that of Lucaogou shale (Hou et al., 2021), another typical lacustrine type-II shale in China. After that, it almost remained the same. For gas yield, the value first increased rapidly with R_o and then increased slowly, showing that it was affected by the cracking of crude oil and wet gas during high evolution stage. However, for samples with TOC $\leq$13.34 wt%, the gas production increased rapidly before $R_o \approx 1.67\%$, and then increased very slowly. While for the two samples with TOC>20 wt%, the trend of increasing gas production was very obvious before $R_o \approx 2.4\%$, and then it showed a gentle increasing trend.

4. Discussions

4.1. Characteristics of the remaining hydrocarbon yield

The hydrocarbons generated but retained in shale, together with the organic matters that were not yet degraded constituted the major source of oil and gas during the in-situ conversion of shale. Subsurface shales have generally undergone thermal evolution.

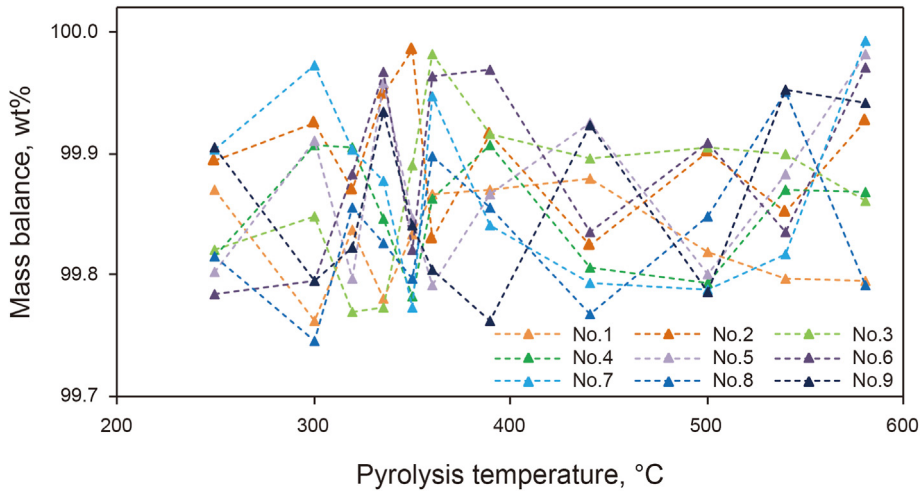

Fig. 3. Evolution of mass fractions of major products with increasing thermal maturity.

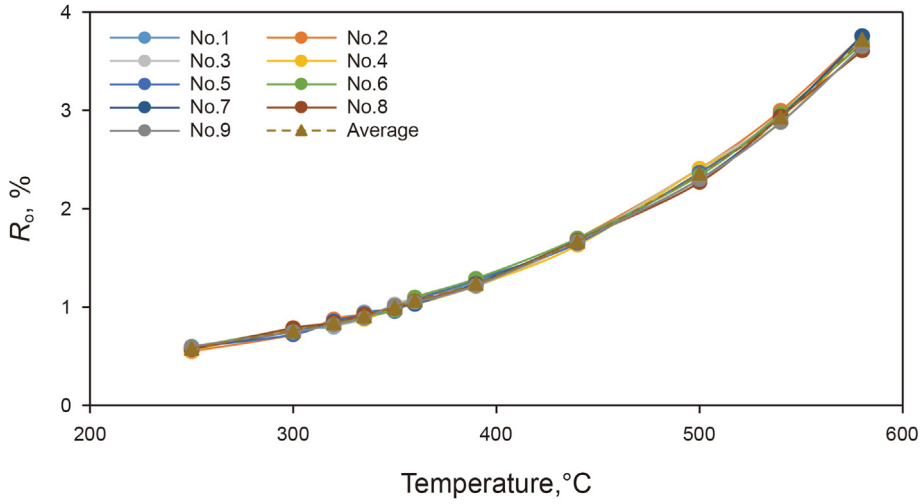

Fig. 4. Correlation between pyrolysis temperature and R_o.

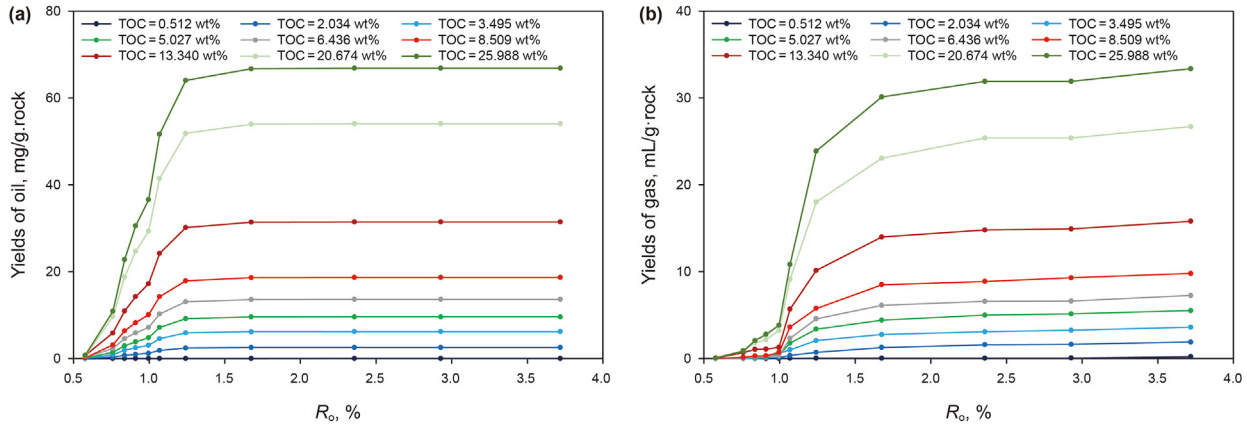

Fig. 5. Yields of oil and gas with increasing R_o. (a) yield of oil, (b) yield of gas.

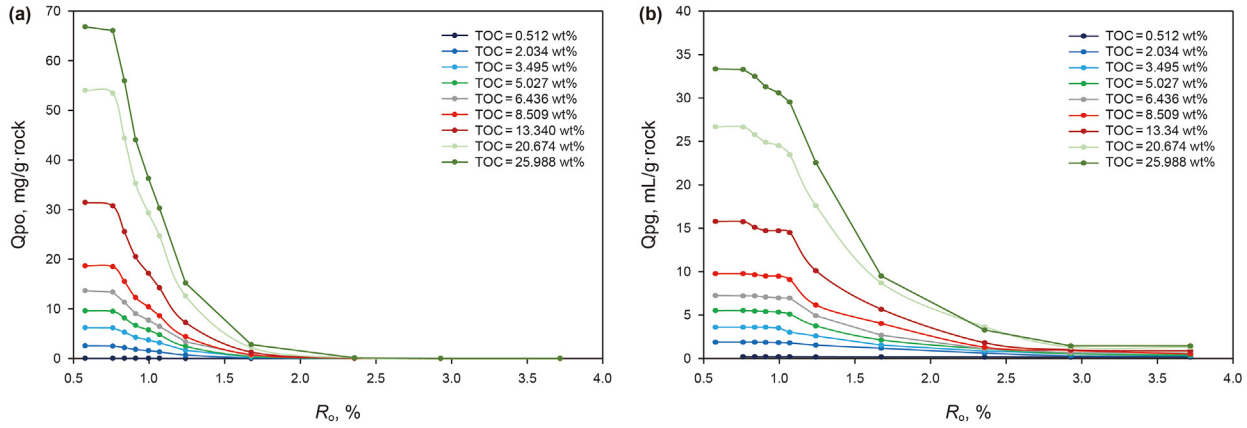

Fig. 6. Yield of the remaining hydrocarbons with increasing R_o. (a) remaining yield of oil, (b) remaining yield of gas.

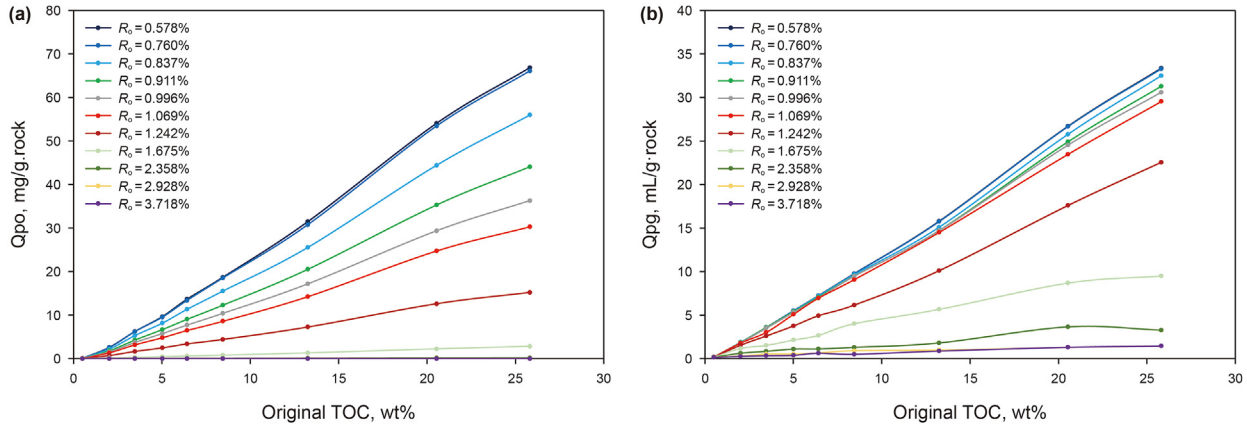

Fig. 7. Yield of remaining hydrocarbons with original TOC. (a) remaining yield of oil, (b) remaining yield of gas.

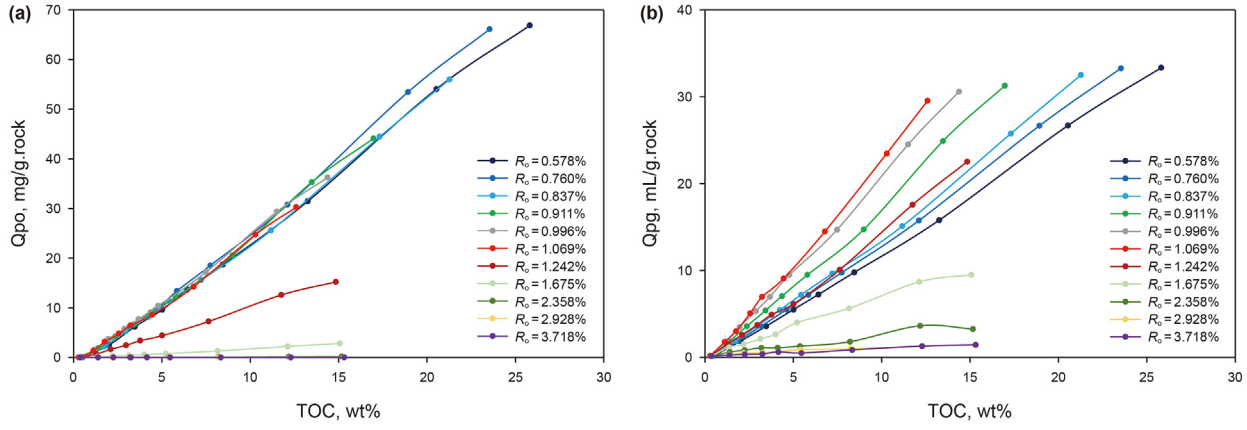

Fig. 8. Yield of remaining hydrocarbons with residual TOC. (a) remaining yield of oil, (b) remaining yield of gas.

Some oil and gas may have been generated and discharged already. Therefore, in this paper, the hydrocarbon yield from in-situ conversion of shale refers to the remaining hydrocarbon yield. With this in mind, we have estimated the hydrocarbon yield from in-situ conversion of shale by calculating the obtained oil and gas at each experimental temperature (yields of the remaining oil and gas are plotted in Fig. 6). It shows that the remaining oil and gas yields exhibit consistent trends as R_o increases and both were negatively correlated with R_o, whereas regarding specific performance, these data reduced slowly at first and then decreased dramatically when R_o reached a certain value. However, oil and gas have different evolution stages. Regarding the remaining oil yield, it decreased slowly when R_o ranged from 0.58% to 0.75%, then it dropped almost linearly when R_o was between 0.75% and 1.25% and decreased slowly again until it reached zero when R_o was greater than 1.25%. In contrast, the remaining gas yield declined slowly when R_o was

from 0.58% to 1.05% and diminished rapidly in a near power function pattern when R_o was between 1.05% and 2.3%. Additionally, the major oil and gas generation stages were different, and it can be concluded from the yield rates that the stage between 0.75% and 1.25% was the major oil generation period, which accounted for 75% of the total oil yield. However, the amount of oil generated during the high evolution stage (R_o 1.7%–2.3%) was small and approached to zero when R_o exceeded 2.3%. On the contrary, the major gas generation period was 1.05%–2.3%. The remaining gas yield declined slowly to a constant level when R_o>2.3%. At this stage, the gas was mainly generated from thermal expansion because of increasing temperature.

TOC was another key factor influencing the potential of shale transformation, as well as R_o. The organic matter provided a material basis for hydrocarbons, and the original TOC in shale determined its ultimate yield of oil and gas. Fig. 7 shows that both the remaining oil yield and gas yield increased with the original TOC for the samples with the same R_o, and there were strong linear correlations between the yield and the original TOC (Fig. 7). Furthermore, the remaining oil yield and gas yield decreased as R_o increased under the same original TOC, which was consistent with previous findings.

When we evaluated the recoverable petroleum resources from in-situ conversion of shale under geologic conditions, we had to understand that the evaluated objects had generally experienced thermal evolution. Because of this, the organic matter in shale had already been transformed making it difficult to obtain the original TOC value. Therefore, the relationship between the remaining oil/gas yield and the residual TOC was a focus in this paper (Fig. 8). The remaining oil yield from shale samples with different TOC values increased as the residual TOC increased when R_o was below 1.7% and changed consistently with TOC when R_o was below 1.1% (Fig. 8a). The remaining gas yield increased as the residual TOC increased when R_o remained the same. However, when TOC was unchanged, the remaining gas yield increased at first and then decreased as R_o increased, and the turning point was at $R_o = 1.1\%$ (Fig. 8b). This feature could be attributed to the evolution process because first, the organic matter generated oil and gas as the temperature rised, then some oil was cracked into coke at high maturity, and these actions caused TOC to decline rapidly at first, then increased slightly, and ultimately remained stable.

Based on the correlations between the remaining oil/gas yield (per mass unit of shale and mass unit of TOC) versus TOC and R_o (Fig. 9a), it could be concluded that, as for the same shale sample, the remaining oil yield increased slightly at first, then decreased steadily and finally diminished rapidly as R_o increased. However, for the remaining gas yield, R_o increased (Fig. 9b).

4.2. Models for evaluating the remaining oil/gas yield from in-situ shale transformation

As previously described, the experimental results demonstrated that there was a strong linear correlation between the remaining oil/gas yield and TOC. Accordingly, a model could be built to express this relationship. Some key parameters were extracted and then used to establish links with R_o, such that a model to evaluate the remaining oil/gas yield with TOC and R_o could be obtained (Equation (3)).

$$Q_{po} = a_1 \times ((e^{a_2 R_O + a_3})TOC - e^{a_4 R_O + a_5}) + a_6 \quad (3)$$

where Qpo is the remaining oil yield per mass unit of shale, R_o is the vitrinite reflectance, and TOC is the total organic carbon. a_1, a_2, a_3, a_4, a_5, and a_6 are empirical parameters, where a_1 and a_6 equal 0.99892 and 0.01538, respectively. When $R_o \le 0.76\%$, a_2 and a_3 equal 0.4265 and 0.7516, when $0.76\% < R_o \le 0.95\%$, a_2 and a_3 equal 0.4593 and 1.41, when $R_o > 0.95\%$, a_2 and a_3 equal 4.164 and 5.3161, when $R_o \le 0.77\%$, a_4 and a_5 equal 0.068 and 1.1297, when $0.77\% < R_o \le 1.06\%$, a_4 and a_5 equal 2.6881 and 3.2629, and when $R_o > 1.06\%$, a_4 and a_5 equal 3.5488 and 4.1449, respectively.

$$Qpg = b_1 \times \begin{cases} (b_2 e^{b_3 R_O})TOC + b_4 \ln R_O + b_5 & R_O \le 0.84\% \\ (b_6 \ln R_O + b_7)TOC + b_8 {R_O}^2 + b_9 R_O + b_{10} & 0.84\% < R_O \le 1.07\% \\ (b_{11} {R_O}^{b_{12}})TOC + b_{13} {R_O}^2 + b_{14} R_O + b_{15} & R_O \ge 1.07\% \end{cases} \quad (4)$$

where Qpg is the remaining gas yield per mass unit of shale, R_o is the vitrinite reflectance, and TOC is the total organic carbon. b_1 to b_{15} are empirical parameters and equal 1.0062, 0.9478, 0.5744, −0.0997, −1.1745, 3.4118, 2.1756, 1.5235, −2.3651, −0.2334, 2.9012, −2.9174, −0.0967, 0.5035, and −0.4776, respectively.

To test the confidence of the models, the remaining oil and gas yields were estimated by Equations (3) and (4) using TOC and R_o data obtained from this study. Through comparisons with experimental results, the correlation coefficients of both the oil and gas yields were greater than 0.997 (Fig. 10). Specifically, the average

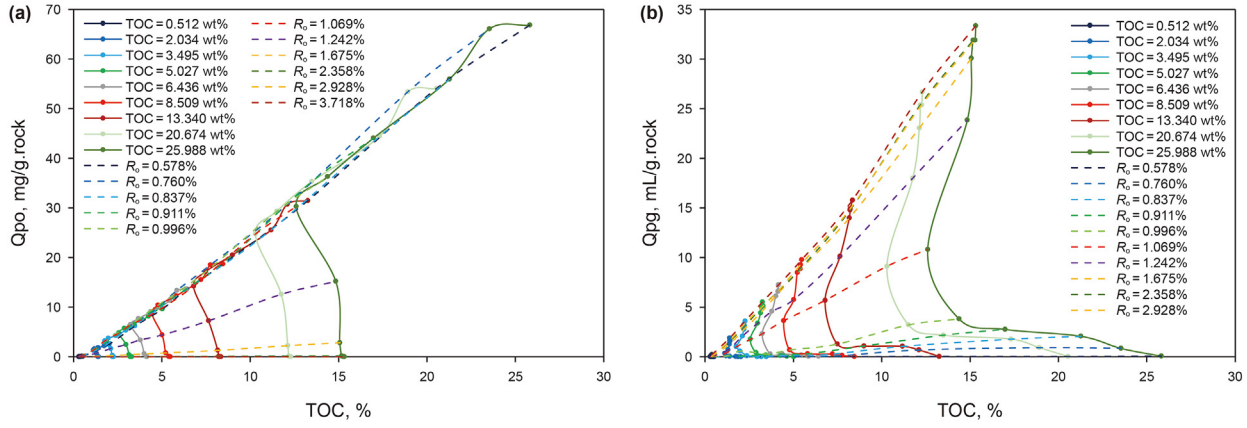

Fig. 9. Yield of remaining hydrocarbons with TOC and R_o. (a) remaining yield of oil, (b) remaining yield of gas.

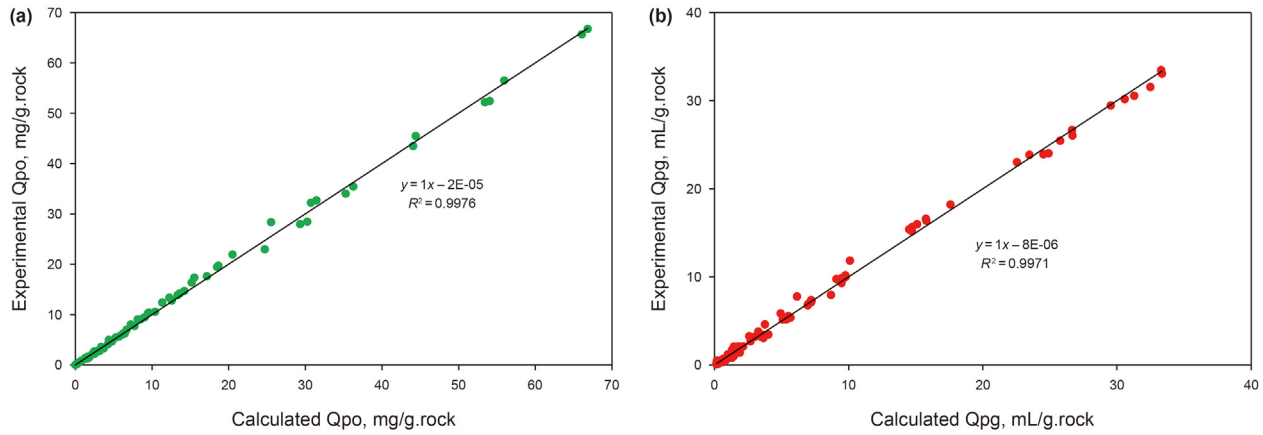

Fig. 10. Relationship between calculated yield and experimental yield. (a) oil yield, (b) gas yield.

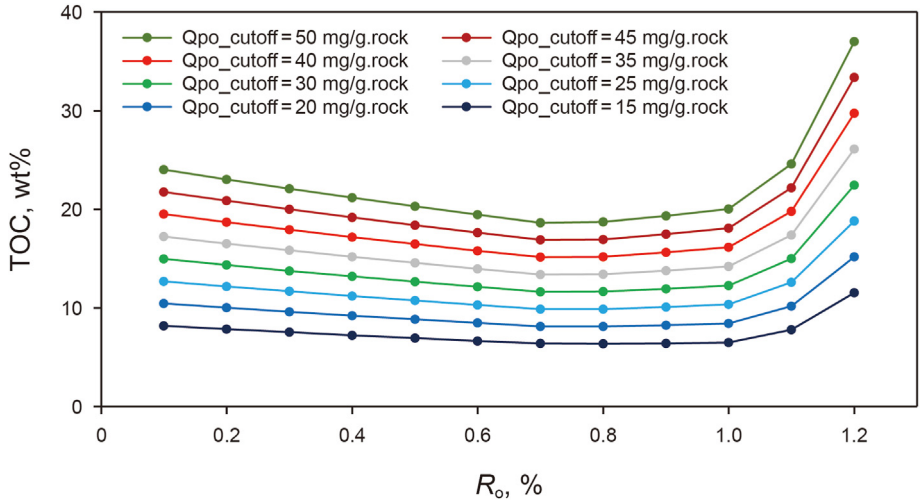

Fig. 11. Relationship of the cutoffs of the remaining oil yield versus R_o and TOC.

absolute error between the calculated remaining oil yield and the experimental yield was 0.0001 mg/g·rock, and the absolute values of the absolute errors averaged 0.4796 mg/g·rock. The average absolute error between the calculated remaining gas yield and the experimental one was −0.0002 m^3/t·rock, and the absolute values of the absolute errors averaged 0.3707 m^3/t·rock. Such figures showed that the models built in this paper were reliable.

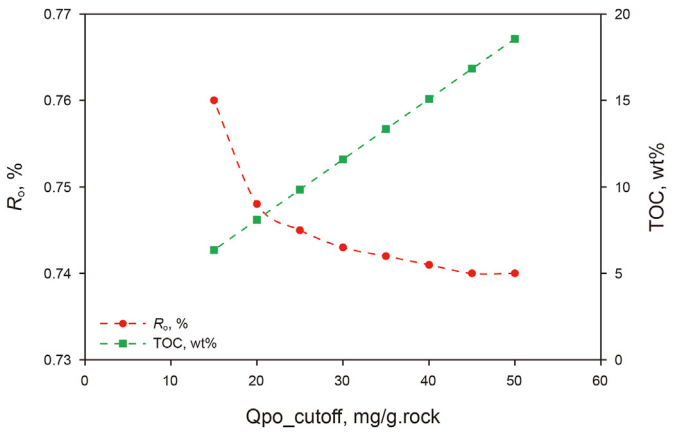

Fig. 12. Relations of the remaining oil yield cutoff versus minimum TOC cutoff and R_o

4.3. Cutoffs of TOC and remaining oil yield

Shale to be developed by in-situ transformation into oil have normally experienced some thermal evolution, and thus, have different remaining oil yields. Furthermore, shale with commercial development value also differs in TOC. Taking the shale samples used in our experiments as an example, the cutoffs of the remaining oil yield of shale were 50 mg/g·rock, 45 mg/g·rock, 40 mg/g·rock, 35 mg/g·rock, 30 mg/g·rock, 25 mg/g·rock, 20 mg/g·rock, and 15 mg/g·rock, respectively. The TOC cutoffs under different R_o values could be obtained by using Equation (1). The results are shown in Fig. 11. When R_o remained unchanged, the TOC cutoff declined as the yield increased. When the cutoff of the remaining oil yield remained the same, the TOC cutoff declined slightly at first and then increased as R_o increased. The minimum value of the TOC cutoff occurred when R_o was approximately 0.75%. Therefore, the shale with R_o of approximately 0.75% offered the best commerciality for development by in-situ transformation, and it was untrue that lower R_o was better. The reasons might be that after oil and/or gas are generated, they are absorbed first by organic matter (Baker,

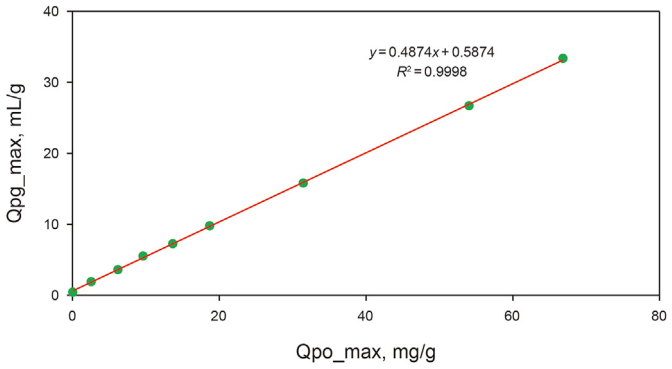

Fig. 13. Relationship between the maximum recoverable oil volume and the maximum recoverable gas volume of the shales.

2016; Tissot et al., 1971; Stainforth and Reinders, 1990; Larsen and Li, 1997; Ertas et al., 2006; Kelemen et al., 2006; Han et al., 2017) and minerals (Schettler and Parmely, 1991; Li et al., 2020). Only when the amount of the generated hydrocarbons is large enough, can microfractures be formed within the source rocks because of increased pressure (Jarvie, 2012), and the oil and/or gas generated from kerogens can then move and be discharged from the source rocks. In summary, the source rock needs to reach a certain maturity to generate enough oil and gas and form an effective hydrocarbon expulsion channel. At this time, the oil and gas generated during in-situ transformation can be directly exploited from shale. As a result, the time to produce oil and/or gas is advanced, which helps to shorten the investment recovery period and improve project economics.

Fig. 12 plots the relationship of the remaining oil yield cutoffs versus minimum TOC cutoffs and R_o, where it can be observed that the minimum TOC cutoff increased as the remaining oil yield cutoff increased, and there was a strong linear correlation between them. In contrast, the R_o corresponding to the minimum TOC cutoff decreased as the cutoff of the remaining oil yield increased. For instance, when the cutoffs of the remaining oil yield were 15 and 50 mg/g·rock, respectively, the R_o values corresponding to the minimum TOC cutoff were 0.76% and 0.74%, respectively.

5. Assessment of recoverable oil and gas resources in Chang 7_3 shale, Ordos Basin

5.1. Geological settings and exploration

The Ordos Basin is located in the central part of North China (Fig. 1), covering an area of approximately 37×10^4 km^2 and contains 146.5×10^8 t and 15.68×10^{12} m^3 of conventional oil and gas resources, respectively. The Triassic Yanchang Formation. and the Jurassic Yan'an Formation are the major oil-bearing series in the basin. The oil source rocks belong to the Yanchang Formation deposited in semi-deep to deep lacustrine facies (Zhang et al., 2006; Li et al., 2019). Specifically, organic-rich shale is mainly developed in the Chang 7_3 section. During the sedimentary period of this section, the maximum water depth of the ancient lake basin could reach 60–120 m, and the distribution area of organic-rich shale is approximately 5×10^4 km^2. By the end of 2019, the total resources in the Ordos Basin were more than 5.6 trillion tons, and the annual oil production was more than 36 million tons. The reservoirs of the Yanchang Formation are tight with low permeability. The average porosity and permeability were 9.9% and 1.23 mD, respectively. Approximately 81.6% of the resources were in reservoirs with a permeability lower than 5 mD, among which 54.3% of the reservoirs featured permeability lower than 1 mD. The estimated ultimate recovery factor of the resources was 15.8%.

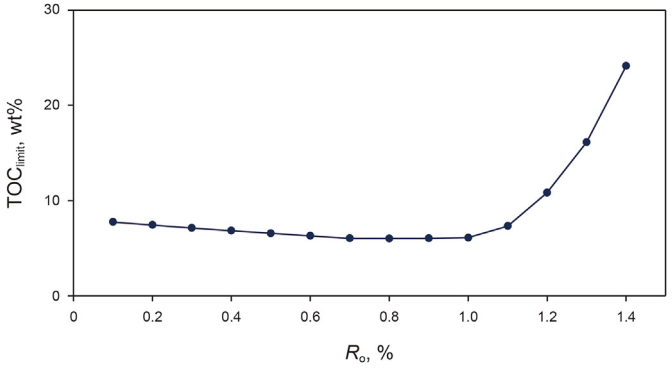

Fig. 14. Scheme of TOC low limit vs R_o.

The Chang 7_3 shale has low maturity with a R_o value average of 0.82%. Tests indicate that it is impossible to realize commercial development using the existing volume fracturing of horizontal wells. The initial oil rates of the seven vertical wells were only 0.60–3.23 t/d after volume fracturing and declined rather rapidly. Taking Well G295 with the slowest decline rate as an example, the daily oil production was 1.09 t/d after producing for 1 year, and the annual oil production was 415.03 t. After producing 912 d, its cumulative oil production was only 623.6 t. All other wells were shut after producing 1–8 months. Estimation of GOR showed that the peak GOR of the Chang 7_3 shale ranged from 60 m^3/m^3 to 98 m^3/m^3, and averaged 83 m^3/m^3. There was liquid petroleum in the shale. In-situ conversion was feasible, although the existing technologies could not realize commercial development.

5.2. Determination of key parameters

The methods for determining the key parameters, such as TOC, R_o, and net pay of shale for assessing the recoverable oil/gas resources from in-situ conversion of shale are introduced in this paper using the Chang 7_3 shale in the Ordos Basin as an example.

5.2.1. Determination of TOC cutoff

To evaluate whether or not the target is economical, it is necessary to determine the cutoffs of recoverable oil and gas volumes of the shale. Because there was a strong linear correlation between the maximum recoverable oil volume and the maximum recoverable gas volume (Fig. 13), it was enough to determine only the cutoff of the recoverable oil volume.

During the commercial development via in-situ shale transformation, the cutoff of recoverable oil volume could be determined with a model (Equation (5)) based on the oil production cutoff of a well group and the mass of the shale in the effective heating area controlled by this group.

$$Q_{\mathrm{po\_limt}} = \frac{Q_{\mathrm{oil\_limt}}}{Wt_{\mathrm{rock}}} \tag{5}$$

Where $Q_{\mathrm{po\_limit}}$ is the cutoff (or lower limit) of recoverable oil volume per mass unit of shale, $Q_{\mathrm{oil\_limit}}$ is the lower limit of the cumulative oil produced by a well group, and Wt_{rock} is the mass of shale in the effective heating area controlled by the well group.

Horizontal wells were used in this paper. Specifically, there were 10 heating wells and one production well in the well group. The spacing between two heating wells was 15 m, and the lateral length of a horizontal well was 1,200 m. Based on these data, the rock mass in the effective heating area was 7,080,000 tons, the cutoff of the oil production was 100,000 tons, and the cutoff of recoverable oil

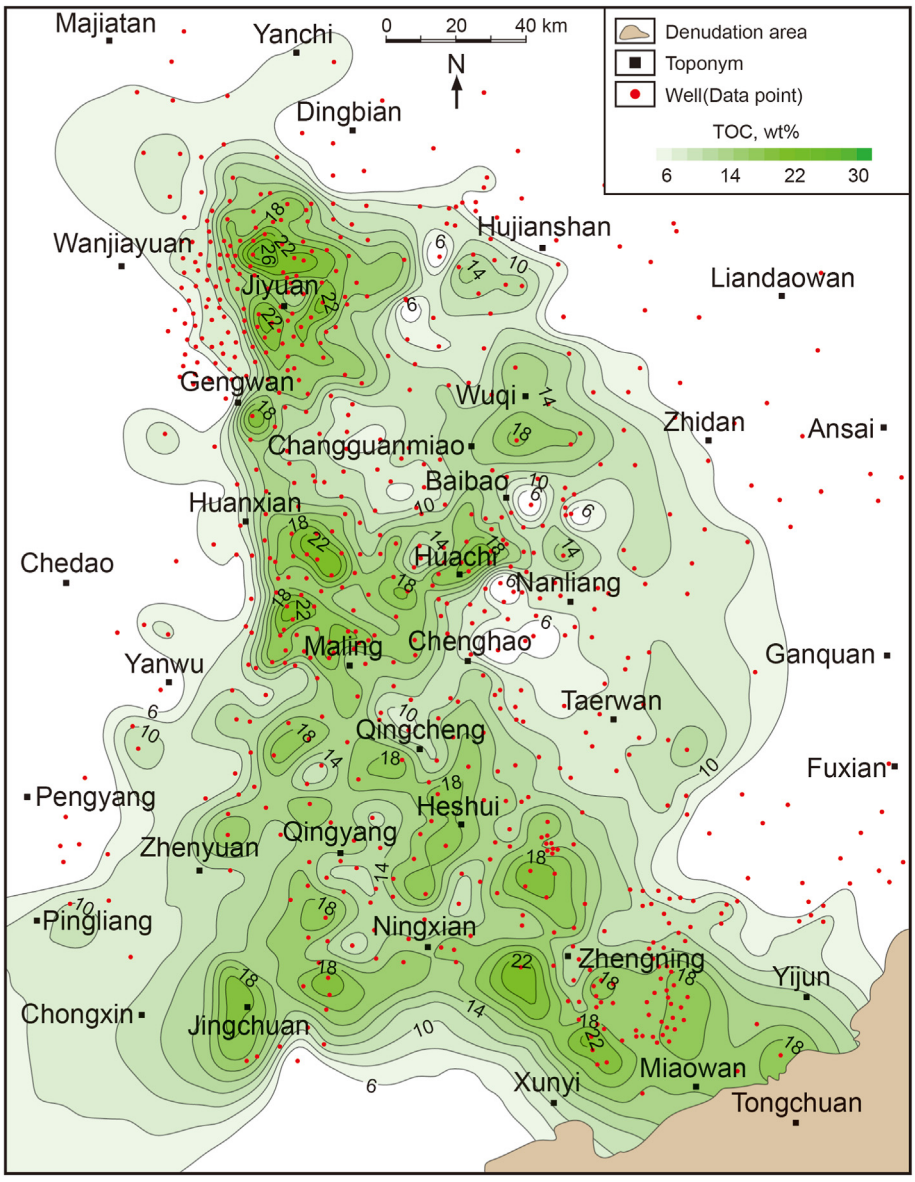

Fig. 15. Distribution of TOC in Chang7_3 of Triassic in Ordos basin.

volume of shale was 14 mg/g·rock as estimated with Equation (5).

The TOC cutoff corresponding to the cutoff of recoverable oil resources per mass unit of shale could be determined with Equation (3) by using the cutoff of recoverable oil volume determined above (Equation (6)).

$$TOC_{\text{limt}} = \frac{c_1 \times Q_{\text{po\_limt}} + e^{c_2 R_o + c_3} + c_4}{e^{c_5 R_o + c_6}} \tag{6}$$

where TOC_{limit} is the TOC lower limit (i.e., cutoff) of the effective shale, $Q_{\text{po\_limit}}$ is the lower limit of recoverable oil volume per mass unit of shale, R_o is the shale to be tested, and c_1, c_2, c_3, c_4, c_5, and c_6 are empirical parameters. c_1 and c_4 are 1.0011 and −0.0154, whereas c_2 and c_3 are 0.068 and 1.1297 when $R_o \leq 0.77\%$, and c_2 and c_3 equal 2.6881 and 3.2629 when $0.775\% < R_o \leq 1.06\%$, and c_2 and c_3 are 3.5488 and 4.1449 when $R_o > 1.06\%$.

Regarding $c5$ and $c6$, they were 0.4265 and 0.7516 when $R_o \leq 0.76\%$, equaled 0.4593 and 1.41 when $0.76\% < R_o \leq 1.0\%$, and they are 4.164 and 5.3161 when $R_o > 1.0\%$.

Assuming the cutoff of recoverable oil volume per mass unit of rock is 14 mg/g·rock, then the plot of R_o versus the TOC_{limit} of the effective shale (Fig. 14) could be obtained using Equation (5), from which it can be seen that the cutoff of TOC is approximately 6% when R_o is approximately 0.8%.

5.2.2. Determination of other key parameters

5.2.2.1. TOC. The analysis of 8690 cores taken from the Chang 7_3 shale from 271 wells indicated that their TOC ranged from 6 to 39 wt%, and averaged 14.32 wt%. In this paper, TOC and R_o obtained from the laboratory tests were used to calibrate the log data using the $\Delta \log R$ method (Passey et al., 1990). Then, the TOC values of the target intervals in 791 wells were obtained by the interpretation model built by zoning. It should be noted that the TOC used here refers to the average TOC of the shale intervals satisfying the TOC cutoff criteria. To test the reliability of the calculation results, referring to the standard of effective shale section, the area and thickness weighted statistics of TOC values in the control area of each well point showed that the variation range was from 6 to

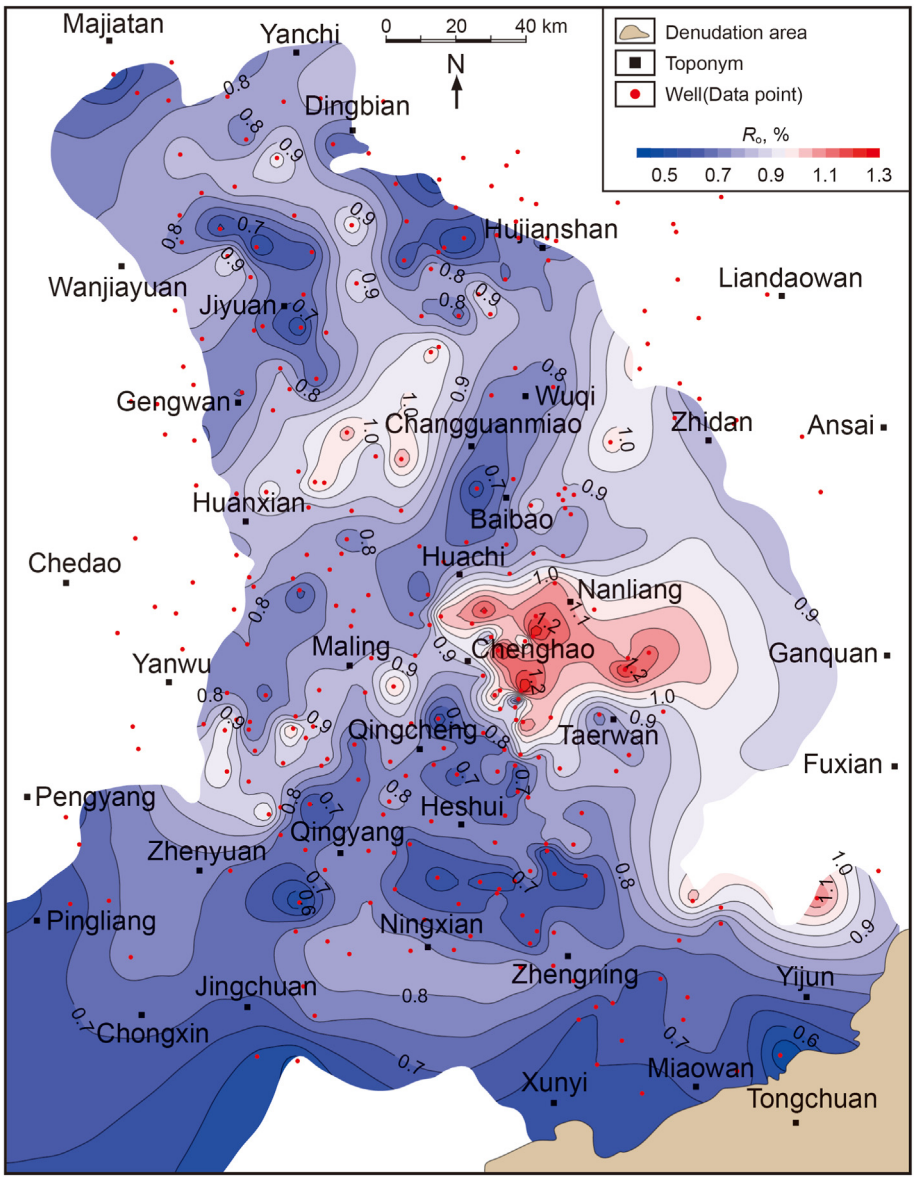

Fig. 16. Distribution of R_o in Chang7_3 of Triassic in Ordos Basin

32.4 wt%, and averaged 14.12 wt%, which was very close to the value obtained from laboratory cores. This result indicated that the calculations were reliable. As Fig. 15 shows, the Chang 7_3 shale with TOC greater than 6 wt% covered an area of approximately 5.1×10^4 km^2, and the organic-rich region (TOC>18 wt%) was mainly distributed in Zhengning–Miaowan, Ningxian–Jingchuan, Heshui–Qingcheng, Maling–Huachi–Changguanmiao, and Maling–Gengwan–Jiyuan. Overall, organic-rich shale sections were distributed in succession, but there was still strong heterogeneity, which reflected the effects of the paleoenvironment on the development of high-quality source rocks. Nevertheless, the Chang 7_3 shale had a good material basis for in-situ transformation.

5.2.2.2. R_o. Altogether, 2200 shale samples were taken from 321 wells to test and analyze the vitrinite reflectance of the Chang 7_3 shale. Based on the analysis results, the R_o distribution map was drawn for the Chang 7_3 shale. According to the results, the Chang 7_3 shale experienced uneven thermal evolution. Its R_o was mainly distributed in 0.52%–1.25%, with an average value of 0.82%. Among these, 93% of the areas had a R_o less than 1.0% and 54.3% had a R_o less than 0.82%; these were mainly distributed in the south of Qincheng, Yanwu–Wuqi, and Gengwan–Yanchi. According to the previous analysis, shales in the above areas have good hydrocarbon generation capacity and should be used as primary targets for in-situ transformation (Fig. 16).

5.2.2.3. Net pay thickness. The effective shale sections suitable for in-situ transformation were divided using the TOC cutoff of effective shale and the TOC value of logging interpretation to obtain the effective shale thickness and determine the favorable shale distribution area. The principles were as follows. ① the TOC of shale was higher than its lower limit value (6 wt%), and the continuous thickness was greater than 2 m; or ② the cumulative thickness of shale section was greater than 2 m, and the accumulated thickness of TOC less than 6 wt% was less than 20% of the thickness of this section, and the single-layer thickness with

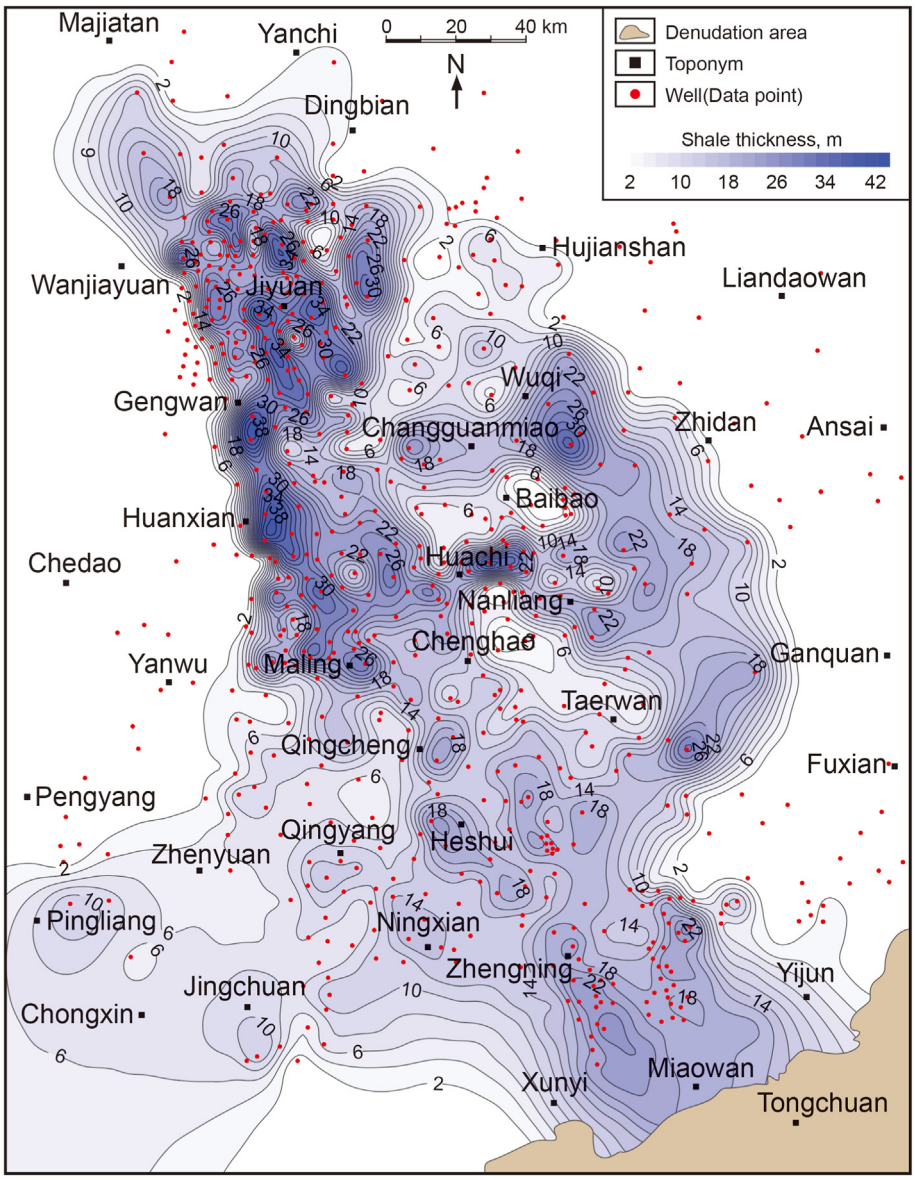

Fig. 17. Distribution of effective shale thickness in the Chang 7_3 of the Triassic in Ordos Basin.

average TOC less than 6 wt% was less than 1 m. According to the above principles, the plane distribution of effective shale thickness of the Chang 7_3 member in the study area was drawn using the logging interpretation results of 791 wells (Fig. 17). The results showed that the effective thickness of the Chang 7_3 shale ranged from 2 m to 49 m, with an average of 17.5 m. Among these, the distribution area with an effective thickness greater than 20 m exceeded 1.5×10^4 km^2 was mainly located in Jiyuan–Maling, the east of Wuqi–Nanliang, and Zhengning–Miaowan, where the average thickness of effective shale is as high as 27.5 m. Additionally, from the profile, the spatial distribution of the effective shale of Chang 7_3 was also very stable, especially in the long axis direction of the paleo deep lake semi-deep lake. The effective shale distribution was continuous and stable, and the thickness change was small (Fig. 18). In the short axis direction, affected by the ancient landform, the effective thickness of the shale changed substantially, but the main body was still relatively continuous with a large thickness (Fig. 19).

5.3. Evaluation method of recoverable oil and gas resources

The recoverable oil and gas resources from in-situ shale transformation were assessed using the following steps: (1) Estimate the remaining oil and gas yield per mass unit of shale through Equations (3) and (4) according to TOC and R_o distribution of effective shale distribution area. (2) Estimate the abundance (or density) of recoverable oil and gas resources in the assessment area by Equations (7) and (8) using the effective shale thickness and shale density (obtained through log data). (3) Estimate the recoverable oil and gas resources based on the control area of evaluation points.

$$AOR = 10^{13} \times Q_{po} \times H_{shale} \times \rho \tag{7}$$

$$AGR = 10^{14} \times Q_{pg} \times H_{shale} \times \rho \tag{8}$$

where AOR is the abundance of recoverable oil resources in the assessment area, AGR is the abundance of recoverable gas resources

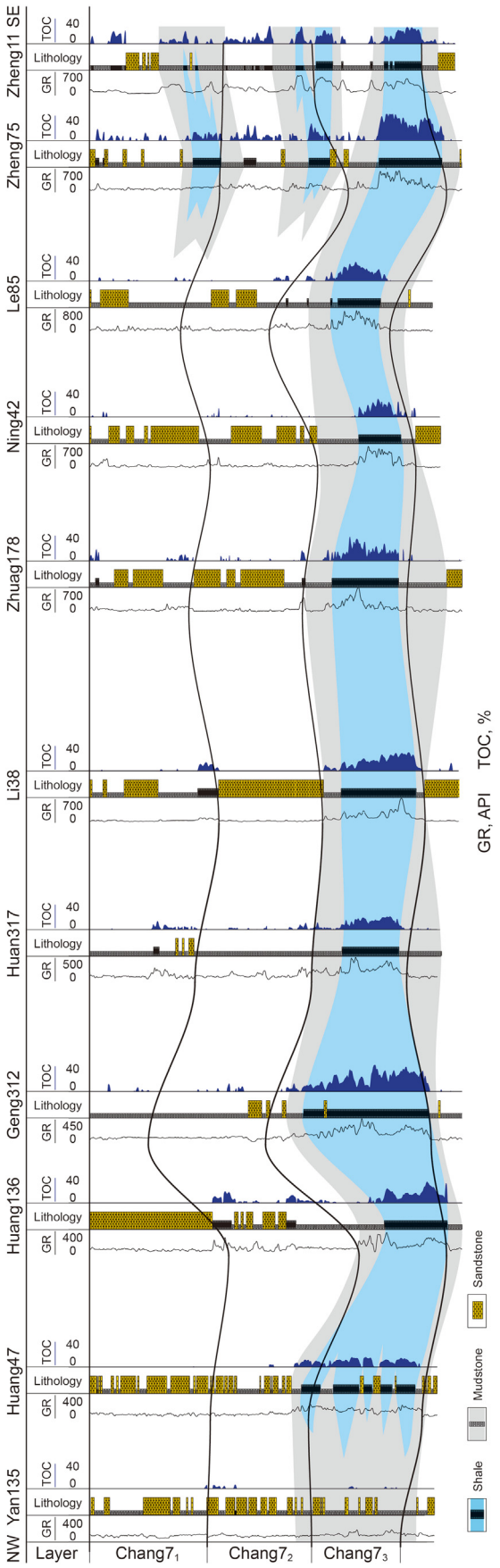

Fig. 18. Organic rich shale section of the Chang7 of Triassic in Ordos Basin (NW-SE) (Location is shown in Fig.1).

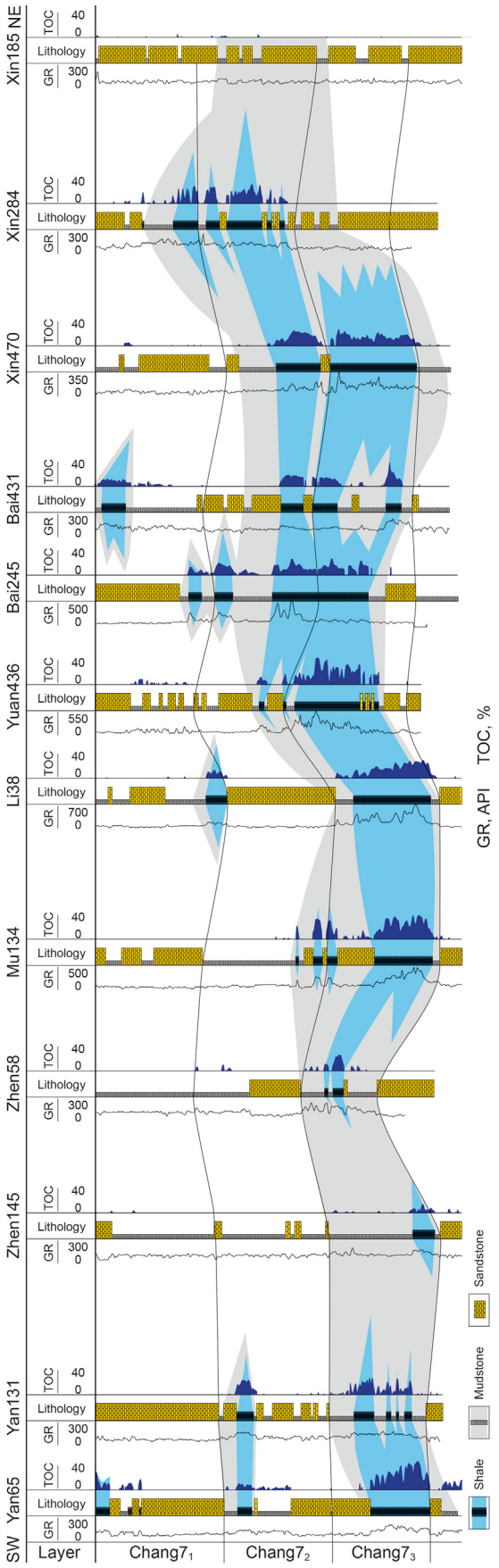

Fig. 19. Organic rich shale section of the Chang7 of Triassic in Ordos Basin (SW-NE) (Location is shown in Fig. 1).

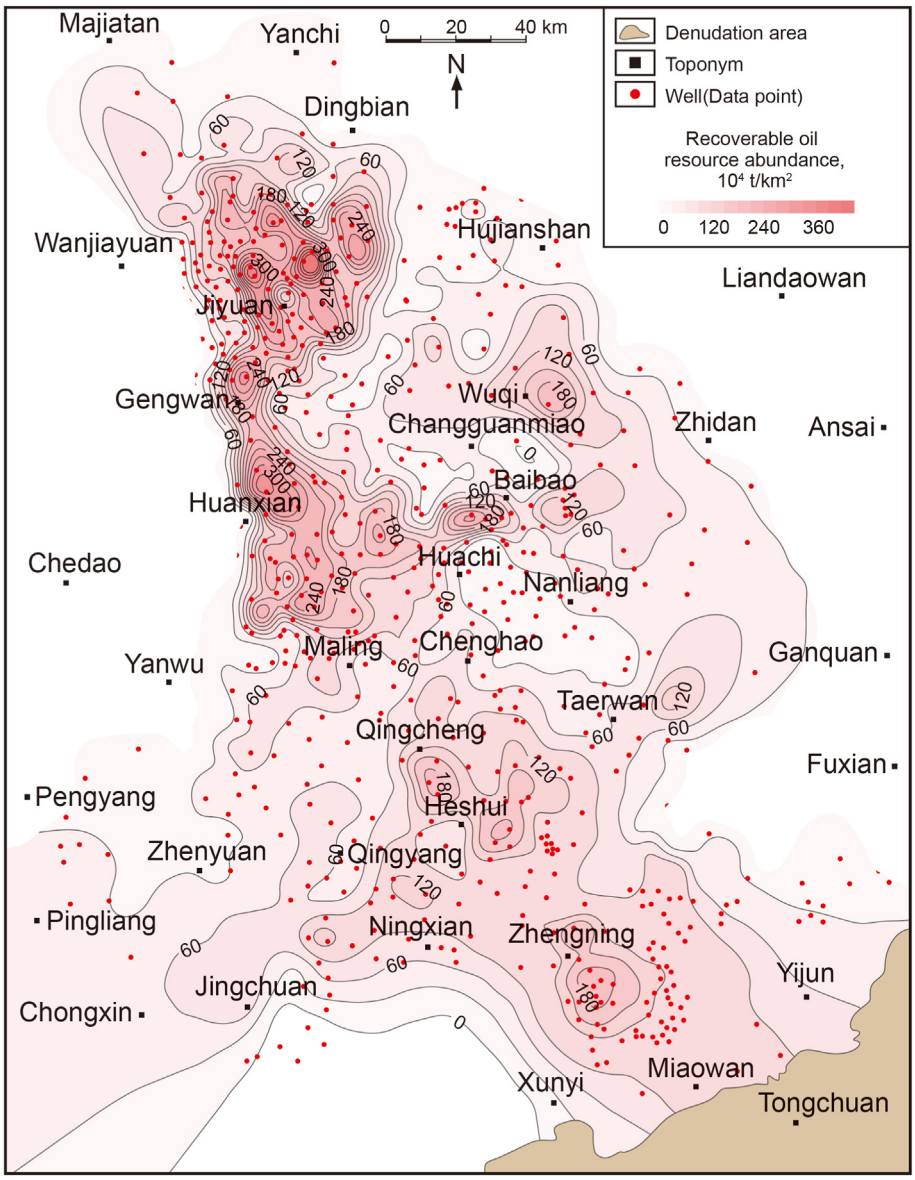

Fig. 20. Distribution of recoverable oil resource abundance in Chang7_3 shale of Triassic in Ordos Basin.

in the assessment area, Q_{po} is the oil recovery volume per mass unit of shale within the effective interval, Q_{pg} is the gas recovery volume per mass unit of shale in the effective interval, and ρ is the shale density in the effective interval.

The evaluation results showed that the recoverable oil resources of the Chang 7_3 shale by in-situ conversion were approximately 450×10^8 t, natural gas was approximately 30×10^{12} m^3, and the distribution area was approximately 4.27×10^4 km^2. The abundance of recoverable oil resources in the effective shale distribution area was 50×10^4 t/km^2–595×10^4 t/km^2, with an average value of 146×10^4 t/km^2. Among these, the area with technically recoverable oil resource abundance greater than 160×10^4 t/km^2 was approximately 1.55×10^4 km^2, mainly distributed in Jiyuan-Gengwan-Maling, Wuqi and Qingcheng-Miaowan (Fig. 20), which were the key areas of the Chang 7_3 shale in-situ conversion. The distribution of recoverable natural gas resource abundance was consistent with this finding. The abundance of recoverable natural gas resources was 3×10^8 m^3/km^2–33×10^8 m^3/km^2, with an average value of 8.1×10^8 m^3/km^2. The area with the resource abundance greater than 8×10^8 m^3/km^2 was approximately 1.66×10^4 km^2, mainly distributed in Jiyuan-Gengwan-Maling, Huachi and Qingcheng-Miaowan (Fig. 21). It was demonstrated that the Chang 7_3 shale in Ordos Basin has a large amount of recoverable oil and gas resources. If it could be effectively utilized, the crude oil production of in-situ transformation could have a resource base of 100 t/year and stable production for more than 100 years.

6. Conclusions

(1) In this paper, the hydrocarbon generation and expulsion process of shale under in-situ conversion were simulated using a large-capacity reactor, slow heating rate, and a semi-open system. It was revealed that TOC and R_o were the key factors affecting the in-situ transformation potential of shale. The remaining oil and gas yield of shale increased linearly with TOC, and the remaining oil yield increased slightly at first and then declined steadily and finally decreased rapidly

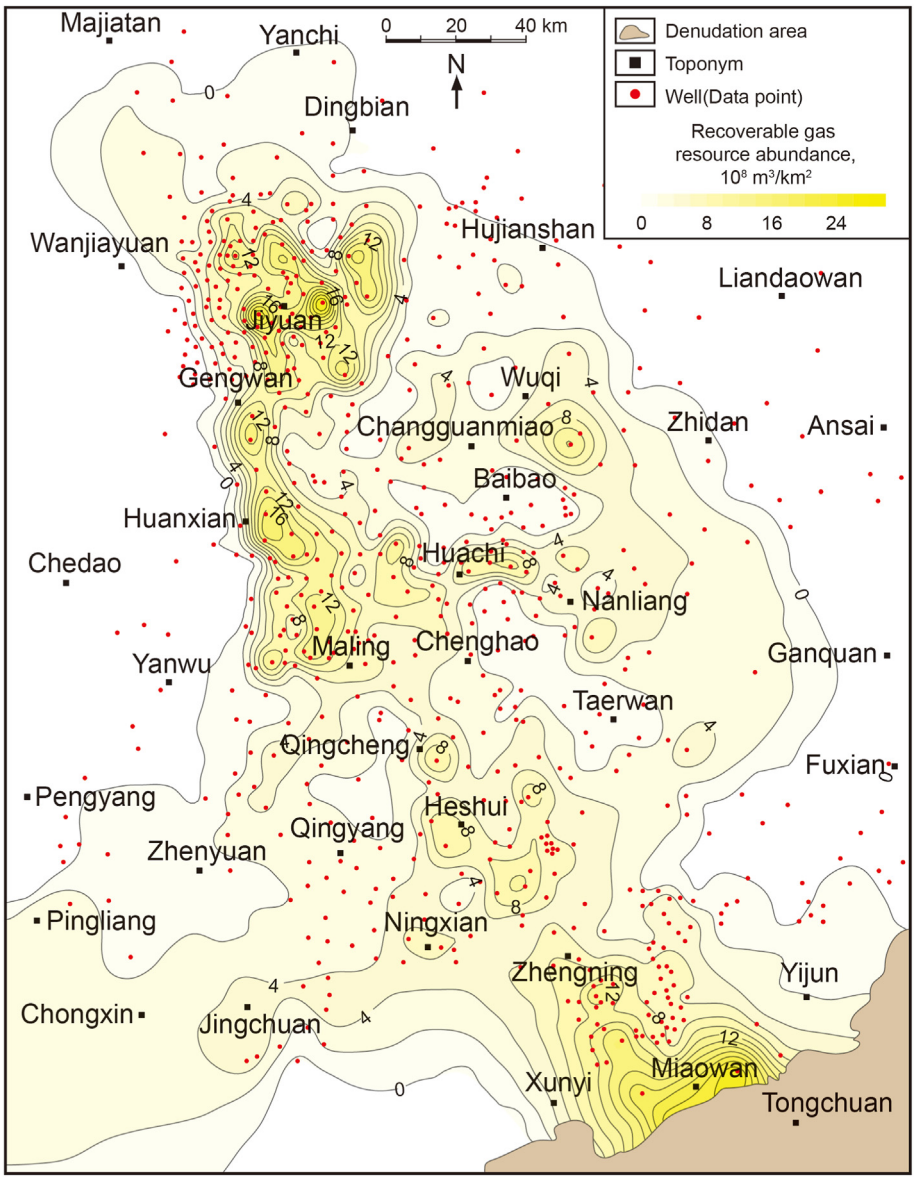

Fig. 21. Distribution of recoverable gas resource abundance in Chang7$_3$ shale of Triassic in Ordos Basin.

as R_o increased; however, the remaining gas yield increased as R_o increased.

(2) R_o ranged 0.75%–1.25% and 1.05%–2.3%, respectively, corresponding to the main oil generation stage and gas generation stage of shale in-situ transformation. The TOC of shale suitable for in-situ conversion should be greater than 6%, whereas its R_o should be less than 1.0%. Shales with 0.75% (R_o) could obtain the best economic benefit. An evaluation model of the remaining oil/gas yield was established.

(3) The organic-rich intervals in the Triassic Chang 7$_3$ shale of the Ordos Basin were characterized as being continuous and having a large thickness and high TOC. They were the optimal targets for in-situ conversion. The resource assessment results of Chang 7$_3$ shale showed that the recoverable oil resources of in-situ transformation were approximately 450×10^8 t, whereas the recoverable gas resources were 30×10^{12} m^3, and the distribution area was approximately 4.27×10^4 km^2. If it could be used effectively, the crude oil output of in-situ transformation in the Ordos Basin has a resource base of 100 t/year and stable production for more than 100 years.

Acknowledgments

This work was supported by PetroChina Co Ltd. (Grant number: 2015D-4810-02; 2018YCQ03; 2021DJ52) and National Natural Science Foundation of China (Grant number: 42172170). We thank the two anonymous reviewers for their valuable suggestions.

References

Bai, F.T., Guo, W., Lü, X.S., et al., 2015. Kinetic study on the pyrolysis behavior of Huadian oil shale via non-isothermal thermogravimetric data. Fuel 146 (15), 111–118. https://doi.org/10.1016/j.fuel.2014.12.073.

Baker, D.R., 2016. Organic geochemistry of Cherokee Group in southeastern Kansas and northeastern Oklahoma. AAPG Bull. 46 (9), 1621–1642. https://doi.org/10.1306/BC7438D9-16BE-11D7-8645000102C1865D.

BP, 2019. BP Statistical Review of World Energy 2019 68th Edition. BP. https://www.bp.com/content/dam/bp/business-sites/en/global/corporate/pdfs/energy-economics/statistical-review/bp-stats-review-2019-full-report.pdf.

Dang, W., Zhang, J.C., Huang, X., et al., 2015. Main-controlling geological factors of gas-bearing property of continental shale gas: a case study of Member 3rd of Shahejie Formation in western Liaohe sag. Acta Pet. Sin. 36 (12), 1516–1530. https://doi.org/10.7623/syxb201512006 (in Chinese).
Doan, T.V.L., Bostrom, N.W., Burnham, A.K., et al., 2013. Green River oil shale pyrolysis: semi-open conditions. Energy Fuels 27 (11), 6447–6459. https://doi.org/10.1021/ef401162p.
Du, J.H., Hu, S.Y., Pang, Z.L., et al., 2019. The types, potentials and prospects of continental shale oil in China. China Pet. Explor. 24 (5), 560–568. https://doi.org/10.3969/j.issn.1672-7703.2019.05.003.
EIA, 2018. Shale in the United States, vol. 10. https://www.eia.gov/energy_in _brief/article/shale in the_united_states.cfm.
EIA, 2019a. Weekly Petroleum Status Report. https://www.eia.gov/petroleum/supply/weekly.
EIA, 2019b. In: International Energy Outlook 2019. https://www.eia.gov/outlooks/ieo.
EIA, 2020-01. Annual Energy Outlook 2020. https://www.eia.gov/outlooks/aeo.
Ertas, D., Kelemen, S.R., Halsey, T.C., 2006. Petroleum expulsion part 1. Theory of kerogen swelling in multicomponent solvents. Energy Fuels 20 (1), 295–300. https://doi.org/10.1021/ef058024k.
Han, X.X., Kulaots, I., Jiang, X.M., et al., 2014. Review of oil shale semicoke and its combustion utilization. Fuel 126 (15), 143–161. https://doi.org/10.1016/j.fuel.2014.02.045.
Han, Y.J., Horsfield, B., Wirth, R., et al., 2017. Oil retention and porosity evolution in organic-rich shales. AAPG Bull. 101 (6), 807–827. https://doi.org/10.1306/09221616069.
Hou, L.H., Ma, W.J., Luo, X., et al., 2020a. Characteristics and quantitative models for hydrocarbon generation-retention-production of shale under ICP conditions: example from the Chang7 member in the Ordos Basin. Fuel 279, 118497. https://doi.org/10.1016/j.fuel.2020.118497.
Hou, L.H., Ma, W.J., Luo, X., et al., 2020b. Chemical structure changes of lacustrine Type-II kerogen under semi-open pyrolysis as investigated by solid-state ^{13}C NMR and FT-IR spectroscopy. Mar. Petrol. Geol. 116, 104348. https://doi.org/10.1016/j.marpetgeo.2020.104348.
Hou, L.H., Ma, W.J., Luo, X., et al., 2021. Hydrocarbon generation-retention-expulsion mechanism and shale oil producibility of the Permian Lucaogou shale in the Junggar Basin as simulated by semi-open pyrolysis experiments. Mar. Petrol. Geol. 125, 104880. https://doi.org/10.1016/j.marpetgeo.2020.104880.
IHS, 2016. Shale & fracking delivered U.S. Energy independence. https://marcellusdrilling.com/2016/06/ihs-report-shale-fracking-delivered-u-s-energy-independence/.
Jarvie, D.M., 2012. Shale resource systems for oil and gas: Part 2—shale-oil resource systems. In: Breyer, J.A. (Ed.), Shale Reservoirs—Giant Resources for the 21st Century, vol. 97. AAPG Memoir, pp. 89–119. https://doi.org/10.1306/13321447M973489.
Jia, C.Z., Zou, C.N., Li, J.Z., et al., 2012. Assessment criteria, main types, basic features and resource prospects of the tight oil in China. Acta Pet. Sin. 33 (3), 343–350. https://doi.org/10.1016/0031-9384(73)90235-7 (in Chinese).
Jin, Z.J., Bai, Z.R., Gao, B., et al., 2019a. Has China ushered in the shale oil and gas revolution? Oil Gas Geol. 40 (3), 451–458. https://doi.org/10.11743/ogg20190301 (In Chinese).
Jin, X., Wang, X.Q., Yan, W.P., et al., 2019b. Exploration and casting of large scale microscopic pathways for shale using electrodeposition. Appl. Energy 247 (1), 32–39. https://doi.org/10.1016/j.apenergy.2019.03.197.
Ju, W., Niu, X.B., Feng, S.B., et al., 2020. Predicting the present-day in situ stress distribution within the Yanchang Formation Chang 7 shale oil reservoir of Ordos Basin, central China. Petrol. Sci. 17, 912–924. https://doi.org/10.1007/s12182-020-00448-8.
Kelemen, S.R., Walters, C.C., Ertas, D., et al., 2006. Petroleum expulsion part 2. Organic matter type and maturity effects on kerogen swelling by solvents and thermodynamic parameters for kerogen fromregular solution theory. Energy Fuels 20 (1), 301–308. https://doi.org/10.1021/ef0580220.
Kuang, L.C., Dong, D.Z., He, W.Y., et al., 2020. Geological characteristics and development potential of transitional shale gas in the east margin of the Ordos Basin, NW China. Petrol. Explor. Dev. 47 (3), 471–482. https://doi.org/10.1016/S1876-3804(20)60066-0.
Lan, X.Z., Luo, W.J., Song, Y.H., et al., 2015. Effect of the temperature on the characteristics of retorting products obtained by yaojie oil shale pyrolysis. Energy Fuels 29, 7800–7806. https://doi.org/10.1021/acs.energyfuels.5b01645.
Larsen, J.W., Li, S., 1997. Changes in the macromolecular structure of a type I kerogen during maturation. Energy Fuels 11 (4), 897–901. https://doi.org/10.1021/ef970007a.
Li, J.L., Zhang, T.S., Jun, Y., et al., 2020. Geochemical characteristics and genetic mechanism of the high-N2 shale gas reservoir in the Longmaxi Formation, Dianqianbei Area, China. Petrol. Sci. 17, 939–953. https://doi.org/10.1007/s12182-020-00456-8.
Li, S., Zhu, R.K., Cui, J.W., et al., 2019. The petrological characteristics and significance of organic-rich shale in the Chang 7 member of the Yanchang Formation, south margin of the Ordos basin, central China. Petrol. Sci. 16, 1255–1269. https://doi.org/10.1007/s12182-019-00386-0.
Lu, S.F., Huang, W.B., Chen, F.W., et al., 2012. Classification and evaluation criteria of shale oil and gas resources: discussion and application. Petrol. Explor. Dev. 39 (2), 268–276. https://doi.org/10.1016/S1876-3804(12)60042-1.
Ma, W.J., Hou, L.H., Luo, X., et al., 2020a. Generation and expulsion process of the Chang 7 oil shale in the Ordos Basin based on temperature-based semiopen pyrolysis: implications for in-situ conversion process. J. Petrol. Sci. Eng. 190, 107035. https://doi.org/10.1016/j.petrol.2020.107035.
Ma, W.J., Hou, L.H., Luo, X., et al., 2020b. Role of bitumen and NSOs during the decomposition process of a lacustrine Type-II kerogen in semi-open pyrolysis system. Fuel 259, 116211. https://doi.org/10.1016/j.fuel.2019.116211.
Ma, W.J., Luo, X., Tao, S.Z., et al., 2020c. Modified pyrolysis experiments and indexes to re-evaluate petroleum expulsion efficiency and productive potential of the Chang 7 shale, Ordos Basin, China. J. Petrol. Sci. Eng. 186, 106710. https://doi.org/10.1016/j.petrol.2019.106710.
Nie, H.K., Jin, Z.J., Bian, R.K., et al., 2016. The "source-cap hydrocarbon-controlling" enrichment of shale gas in upper ordovician wufeng formation-lower silurian longmaxi formation of sichuan Basin and its periphery. Acta Pet. Sin. 37 (5), 557–571. https://doi.org/10.7623/syxb201605001 (In Chinese).
Passey, Q.R., Creaney, S., Kulla, J.B., et al., 1990. A practical model for organic richness from porosity and resistivity logs. AAPG Bull. 74 (12), 1777–1794. https://doi.org/10.1306/0C9B25C9-1710-11D7-8645000102C1865D.
Perrin, J., 2019-06-06. Horizontally Drilled Wells Dominate U.S. Tight Formation Production. https://www.eia.gov/todayinenergy/detail.php?id=39752.
Saif, T., Lin, Q.Y., Butcher, A.R., et al., 2017. Multi-scale multi-dimensional microstructure imaging of oil shale pyrolysis using X-ray micro-tomography, automated ultra-high resolution SEM, MAPS Mineralogy and FIB-SEM. Appl. Energy 202, 628–647. https://doi.org/10.1016/j.apenergy.2017.05.039.
Schettler Jr., P.D., Parmely, C.R., 1991. Contributions to Total Storage Capacity in Devonian Shales: SPE Eastern Regional Meeting. Kentucky, Lexington October, pp. 22–25. https://doi.org/10.2118/23422-MS.
Shao, D.Y., Zhang, T.W., Ko, L.T., et al., 2019. Empirical plot of gas generation from oil-prone marine shales at different maturity stages and its application to assess gas preservation in organic-rich shale system. Mar. Petrol. Geol. 102, 258–270. https://doi.org/10.1016/j.marpetgeo.2018.12.044.
Siramard, S., Bunman, Y., Lai, D.G., et al., 2017. Pyrolysis of huadian oil shale in an infrared heating reactor. Energy Fuels 31, 6996–7003. https://doi.org/10.1021/acs.energyfuels.7b00964.
Song, M.S., Liu, H.M., Wang, Y., et al., 2020. Enrichment rules and exploration practices of paleogene shale oil in jiyang depression, bohai bay basin. China. Pet. Explor. Dev. 47 (2), 242–253. https://doi.org/10.1016/S1876-3804(20)60043-X.
Stach, E.M., Mackowsky, T.M., Teichmuller, G.H., et al., 1982. Stach's Textbook of Coal Petrology. Gebruder Borntraeger, Berlin, p. 535.
Stainforth, J.G., Reinders, J.E.A., 1990. Primary migration of hydrocarbons by diffusion through organic matter networks, and its effect on oil and gas generation. Org. Geochem. 16 (1–3), 61–74. https://doi.org/10.1016/0146-6380(90)90026-V.
Sun, J., Xiao, X.M., Cheng, P., et al., 2019. Formation and evolution of nanopores in shales and its impact on retained oil during oil generation and expulsion based on pyrolysis experiments. J. Petrol. Sci. Eng. 176, 509–520. https://doi.org/10.1016/j.petrol.2019.01.071.
Tang, X., Zhang, J.C., Jin, Z.J., et al., 2015. Experimental investigation of thermal maturation on shale reservoir properties from hydrous pyrolysis of Chang 7 shale, Ordos Basin. Mar. Petrol. Geol. 64, 165–172. https://doi.org/10.1016/j.marpetgeo.2015.02.046.
Tissot, B.P., Califet-Debyser, Y., Deroo, G., et al., 1971. Origin and evolution of hydrocarbons in early Toarcian shales, Paris Basin, France. AAPG Bull. 55 (12), 2177–2193. https://doi.org/10.1306/819A3E2E-16C5-11D7-8645000102C1865D.
Tissot, B.P., Welte, D.H., 1984. Petroleum Formation and Occurrence, second ed. SpringerVerlag, Berlin.
Wang, Y.P., Wang, Y.W., Meng, X.L., et al., 2013. Enlightenment of American oil shale in-situ retorting technology. Oil Drill. Prod. Technol. 35 (6), 55–59 (In Chinese).
Xue, H.T., Tian, S.S., Lu, S.F., et al., 2015. Selection and verification of key parameters in the quantitative evaluation of shale oil: a case study at the qingshankou Formation,Northern Songliao basin. Bull. China Soc. Mineral Petrol. Geochem. 34 (1), 70–78 (In Chinese).
Yan, G., Xu, Y.H., Liu, Y., et al., 2019. Evolution and organic geochemical significance of bicyclic sesquiterpanes in pyrolysis simulation experiments on immature organic-rich mudstone. Petrol. Sci. 16, 502–512. https://doi.org/10.1007/s12182-019-0326-6.
Yang, L., Jin, Z.J., 2019. Global shale oil development and prospects. China Pet. Explor. 24 (5), 553–559. https://doi.org/10.3969/j.issn.1672-7703.2019.05.002 (in Chinese).
Yang, Z., Zou, C.N., 2019. Exploring petroleum inside source kitchen": connotation and prospects of source rock oil and gas. Petrol. Explor. Dev. 46 (1), 183–193. https://doi.org/10.1016/S1876-3804(19)30018-7.
You, Y.L., Han, X.X., Wang, X.Y., et al., 2019. Evolution of gas and shale oil during oil shale kerogen pyrolysis based on structural characteristics. J. Anal. Appl. Pyrolysis 138, 203–210. https://doi.org/10.1016/j.jaap.2018.12.025.
Zendehboudi, S., Bahadori, A., 2017. Chapter 7: Production Methods in Shale Oil Reservoir. Shale Oil and Gas Handbook. Elsvier, Amsterdam, pp. 285–319.
Zhao, W.Z., Dong, D.Z., Li, J.Z., et al., 2012. The resource potential and future status in natural gas development of shale gas in China. Strategic Study of CAE 14 (7), 46–52 (In Chinese).
Zhao, W.Z., Hu, S.Y., Hou, L.H., 2018a. Connotation and strategic role of in-situ conversion processing of shale oil underground in the onshore China. Petrol. Explor. Dev. 45 (4), 563–572. https://doi.org/10.1016/S1876-3804(18)30063-6.
Zhao, W.Z., Hu, S.Y., Hou, L.H., et al., 2020. Types and resource potential of continental shale oil in China and its boundary with tight oil. Petrol. Explor. Dev. 47 (1), 1–11. https://doi.org/10.1016/S1876-3804(20)60001-5.

Zhao, W.Z., Li, J.Z., Yang, T., et al., 2016. Geological difference and its significance of marine shale gases in South China. Petrol. Explor. Dev. 43 (4), 547–559. https://doi.org/10.1016/S1876-3804(16)30065-9.

Zhang, W.Z., Yang, H., Li, J.F., et al., 2006. Leading effect of high-class source rock of Chang 7 in Ordos Basin on enrichment of low permeability oil-gas accumulation——hydrocarbon generation and expulsion mechanism. Petrol. Explor. Dev. 33 (3), 289–293 (In Chinese).

Zhao, X.Z., Zhou, L.H., Pu, X.G., et al., 2018b. Geological characteristics of shale rock system and shale oil exploration breakthrough in a lacustrine basin: a case study from the paleogene 1st sub-member of kong 2 member in cangdong sag, bohai bay basin, China. Petrol. Explor. Dev. 45 (3), 377–388. https://doi.org/10.1016/S1876-3804(18)30043-0.

Zhou, Q.F., Jin, Z.J., Yang, G.F., et al., 2019. Shale oil exploration and production in the U.S.: status and outlook. Oil Gas Geol. 40 (3), 469–477 (In Chinese).

Zou, C.N., Dong, D.Z., Wang, S.J., et al., 2010. Geological characteristics and resource potential of shale gas in China. Petrol. Explor. Dev. 37 (6), 641–653. https://doi.org/10.1016/S1876-3804(11)60001-3.

Zou, C.N., Dong, D.Z., Yang, H., et al., 2011. Conditions of shale gas accumulation and exploration practices in China. Nat. Gas. Ind. 31 (12), 26–39. https://doi.org/10.4028/www.scientific.net/AMR.978.161 (in Chinese).

Zou, C.N., Pan, S.Q., Jing, Z.H., et al., 2020. Shale oil and gas revolution and its impact. Acta Pet. Sin. 41 (1), 1–12 (In Chinese).

Zou, C.N., Yang, Z., Dai, J.X., et al., 2015. The characteristics and significance of conventional and unconventional Sinian–Silurian gas systems in the Sichuan Basin, central China. Mar. Petrol. Geol. 64, 386–402. https://doi.org/10.1016/j.marpetgeo.2015.03.005.

Zou, C.N., Yang, Z., Wang, H.Y., et al., 2019. “Exploring petroleum inside source kitchen”: Jurassic unconventional continental giant shale oil & gas field in Sichuan basin, China. Acta Geol. Sin. 93 (7), 1551–1562 (In Chinese).